

Pulse interaction via gain and loss dynamics in passive mode locking

Michel Nizette^{a,*}, Dmitrii Rachinskii^b, Andrei Vladimirov^c, Matthias Wolfrum^c

^a *Université Libre de Bruxelles, Theoretical Nonlinear Optics C.P. 231, Bd. du Triomphe, B-1050 Brussels, Belgium*

^b *Department of Applied Mathematics, University College Cork, Ireland*

^c *Weierstrass Institute for Applied Analysis and Stochastics, Mohrenstrasse 39, D-10117 Berlin, Germany*

Received 3 November 2005; received in revised form 6 March 2006; accepted 22 April 2006

Available online 26 May 2006

Communicated by J. Lega

Abstract

We study theoretically the effects of pulse interactions mediated by the gain and absorber dynamics in a passively mode-locked laser containing a slow saturable absorber, and operating in a regime with several pulses coexisting in the cavity.

© 2006 Elsevier B.V. All rights reserved.

Keywords: Lasers; Mode locking; Bifurcations; Pulse interaction; Q-switching

1. Introduction

Passive mode locking provides a very effective technique for generating short laser pulses with high quality and fast repetition rate. The basic mechanism for pulse amplification is the opening of a short temporal window of net gain due to the dynamic interplay of a gain medium and a saturable absorber inside the laser cavity [1]. This mechanism is well understood since the analyses by New [2] and Haus [3] from simple models, which could be handled analytically.

The fundamental mode-locking regime corresponds to a single light pulse that travels round the laser cavity and hits the output mirror periodically. This results in pulse emissions with intervals equal to the round-trip time in the cavity. Operation with multiple coexisting pulses has also been reported, either of bound states of tightly packed pulses [4–11], or as pulse trains with a separation much larger than the pulse width. The formation of bound states was attributed to the interaction of acoustic modes with light pulses [12] and to the coherent pulse interactions via their fast decaying tails [13,14]. In the case of widely separated pulses, they can be either irregularly spaced [5,15–17] or form equally spaced sequences

which were observed in soliton lasers [18–21], semiconductor lasers coupled to an external cavity [22], and monolithic semiconductor lasers [23]. Such equidistant sequences of pulses are in any case easily achieved by using active modulation [18, 19,24–26]. The regimes with two and more equally spaced mode-locked pulses in the cavity is usually referred to as harmonic mode locking. These regimes are characterized by a pulse repetition rate that is a multiple of that of the fundamental mode-locking regime.

The existence of regular, widely spaced, passively mode-locked multiple-pulse regimes was described in [27] by a simple analytical model based on energy rate equations. It was shown that two- or n -pulse operation is favored over single pulse operation when the “dynamic gain” for the multi-pulse state is greater than that of the single-pulse one. The Q-switching instability of mode-locked solutions, which leads to a modulation of the envelope of the pulse train with a frequency that is typically much smaller than the mode-locking frequency itself, can also be described within the framework of simple rate equations [28]. A similar approach based on energy balance considerations was used in [5] to describe an instability leading to the transition from a single pulse to a multi-pulse operation in a solid state laser. However, the understanding of the mechanisms that lead to pulse ordering in the cavity and to the corresponding time scales is challenging, because they can be influenced by many different physical effects that can take place in a mode-locked laser. The associated mathematical

* Corresponding author. Tel.: +32 2 650 58 22.

E-mail addresses: mnizette@ulb.ac.be (M. Nizette), D.Rachinskii@ucc.ie (D. Rachinskii), vladimir@wias-berlin.de (A. Vladimirov), wolfrum@wias-berlin.de (M. Wolfrum).

models all have their strengths, weaknesses, and limited validity. Nevertheless, an investigation of these mechanisms within different mathematical frameworks is valuable, because the question is relevant to the production of pulse trains with higher repetition rates, or by means of longer cavities, for optical communication systems.

As soon as multiple pulses coexist in the cavity, they can interact. The purpose of this work is to explore theoretically the consequences of pulse interactions via the gain and absorber dynamics on the stability of regimes of operation with multiple, well-separated, evenly spaced pulses. To this end, we consider a model for passive mode locking that is almost as simple as the classical models by New [2] and Haus [3], except that it is free from the usual approximations of small gain per cavity round-trip and weak saturation. This is a necessary feature for our purposes, because stable multiple-pulse operation tends to appear only beyond a certain level of pumping above the lasing threshold [5]. We thus need a model that remains valid for high pulse intensities, which potentially requires a high gain per cavity round-trip and induces strong gain and absorber depletions. Otherwise, for the sake of simplicity, we keep the description of the physics inside the laser as elementary as possible.

The paper is organized as follows. In [Section 2](#), we introduce the model and mention the main simplifications involved. [Section 3](#) presents bifurcation diagrams computed by direct numerical integration of the model and points out a number of differences in the stability properties of single-pulse and multiple-pulse regimes. In [Section 4](#), we discuss one particular instability of a two-pulse configuration that manifests itself as a sudden jump towards the single-pulse solution as the gain pumping is gradually decreased towards the lasing threshold. We give evidence that the jump and the associated transient oscillatory dynamics result from pulse interactions mediated by the gain and absorber dynamics. In [Section 5](#), we proceed to an asymptotic analysis of the model based on the identification of several well-separated time scales. This provides some necessary background for the two next sections, where we determine how the pulse interactions depend on their separation distance. In [Section 6](#), we consider the case where the laser operates close to threshold, and do a local analysis in the vicinity of some relevant codimension-2 point. We find that, according to our model, two-pulse solutions emerge unstable at the lasing threshold, and thus must stabilize through a secondary bifurcation located outside the domain of validity of the local analysis. In [Section 7](#), by means of a global analysis, we find the bifurcation and identify it as the cause for the abrupt jump to single-pulse solutions mentioned above. At the critical point, the branch of equally spaced two-pulse solutions connects to an unstable limit cycle created by the interplay of a fast pulse energy relaxation dynamics and a slow pulse displacement dynamics resulting from the pulse interactions. Based on this mechanism, we explain a scaling law that exists between the period of the transient oscillations during the jump and the pulse width. Conclusions are given in [Section 8](#) and contrasted to [29], where a stabilization of multiple-pulse configurations due to pulse interactions in a passively

mode-locked laser with a Kerr nonlinearity is predicted using a theory valid near the lasing threshold.

2. Model

Our model for passive mode locking was derived in [30] using a lumped element approach. We consider an optical cavity containing a gain medium, a passive saturable absorber, and a thin spectral filtering element whose purpose is to limit the frequency bandwidth of the laser radiation. We assume a ring cavity geometry, with one of the counter-propagating waves suppressed so that the lasing is unidirectional. With the additional assumption of a Lorentzian profile for the spectral filter, the model is given by the following system of delay-differential equations for the electric field amplitude A at the entrance of the absorber medium, the saturable gain g , and the saturable absorption level q as functions of time t :

$$\left(1 + \gamma^{-1} \frac{d}{dt}\right) A = \sqrt{\kappa} \exp\left\{\frac{1}{2} [g(t-T) - q(t-T)]\right\} \times A(t-T), \quad (1a)$$

$$\frac{dg}{dt} = \gamma_g (G_0 - g) - \exp(-q) [\exp(g) - 1] A^2, \quad (1b)$$

$$\frac{dq}{dt} = \gamma_q (Q_0 - q) - s [1 - \exp(-q)] A^2. \quad (1c)$$

The two control parameters are the unsaturated gain G_0 and absorber level Q_0 . The other model parameters are the cavity's attenuation factor per round-trip κ , the cold-cavity round-trip time T , the spectral filter width γ (which limits the minimum width of the pulses), the gain and absorber recovery rates γ_g and γ_q , and the ratio s of the saturation energies of the gain and absorber media. Eqs. (1) are equivalent to the model derived in [30] with $g_0 \equiv \gamma_g G_0$, $q_0 \equiv \gamma_q Q_0$, $a \equiv \sqrt{E_g} A$, and the amplitude-phase coupling constants α_g and α_q set to zero.

The model (1) neglects spatial effects associated with linear cavity design, as well as any phase dynamics (since in the absence of α factors the solutions of the field equation (1a) have a fixed phase). The present analysis can be extended to the full model derived in [30], which provides an accurate description of a semiconductor laser (as it holds under conditions of strong saturation and accounts for amplitude–phase coupling).

3. Bifurcation diagrams

Depending on the parameter values, Eq. (1) can exhibit various dynamical regimes, including chaotic behavior. However, most important from the practical viewpoint are the regimes characterized by periodic trains of regularly spaced mode-locked pulses. As illustrated schematically in [Fig. 1](#), mode-locking regimes can have different repetition rates, which are proportional to the number of pulses emitted within the cavity round-trip time. The fundamental mode-locking regime is characterized by the emission of a single pulse per cavity round-trip, while harmonic mode-locking regimes correspond to pulse repetition rates equal to integer multiples of the fundamental repetition rate. Inside each of the emission patterns shown in [Fig. 1](#), all pulses are identical and equidistant.

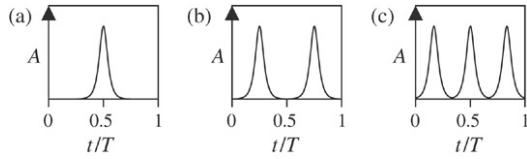


Fig. 1. Regular pulse train solutions of Eq. (1): (a) fundamental regime, with a pulse being emitted after every cavity round-trip; (b) second harmonic, with twice the fundamental repetition rate; (c) third harmonic, with tripled repetition rate.

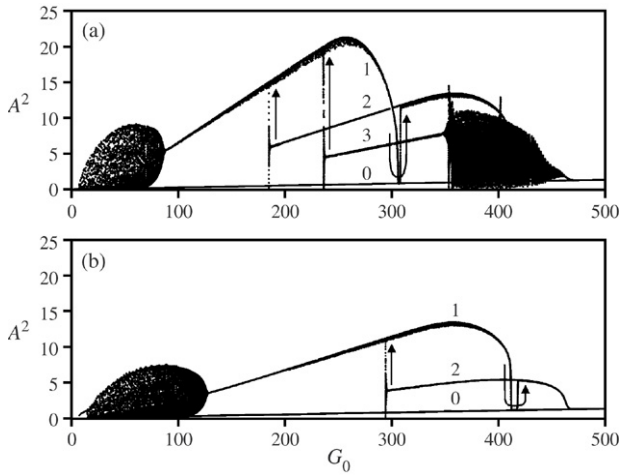


Fig. 2. Maxima of the laser intensity A^2 as a function of the unsaturated gain G_0 , computed by direct numerical integration of Eqs. (1). The solution branches labeled 1, 2, and 3 correspond to regular pulse trains with the fundamental repetition rate and its second and third harmonics, respectively. The branch labeled 0 corresponds to CW emission. Fixed parameter values are $Q_0 = 4$, $\kappa = 0.1$, $\gamma = 100$, $\gamma_g = 0.025$, $\gamma_q = 1.875$, $s = 25$, and (a) $T = 1$, (b) $T = 0.5$ (dimensionless units).

The domains of existence of different mode-locking regimes can overlap in parameter space. Fig. 2 shows two typical bifurcation diagrams for the case of a slow absorber where the relaxation time of the absorber is much longer than the duration of a pulse. They have been obtained by slowly sweeping the value of the unsaturated gain parameter G_0 back and forth so as to explore the whole domains of stability of several branches of pulsed emission regimes. For all solutions with non-stationary electric field envelope, only the maxima of the light intensity time dependence are shown. The branch of CW regime, which is unstable for the most part, is labeled 0 in Fig. 2.

In Fig. 2(a), three branches of pulsed regimes can be distinguished, corresponding to the periodic pulse trains with one, two, and three emitted pulses per cavity round-trip. These regimes are similar to those illustrated by Fig. 1. As the control parameter is swept back and forth, the various branches of periodic pulse trains suffer various kinds of transitions and instabilities. The single-pulse emission domain is limited to the right by a gradual shrinking of the pulse peak intensity to the CW level, indicating the collapse of the pulsed regime onto the unstable steady state. This event is quickly followed by a transition to the two-pulse branch, which itself eventually undergoes a similar collapse. In addition, two instabilities

leading to non-uniform pulse trains can be observed in Fig. 2(a). One of them lies around $G_0 \simeq 350$ and involves a transition to a quasiperiodic solution with four pulses per round-trip. The other lies on the single-pulse branch, at $G_0 \simeq 90$, and can be identified as a Q-switching instability [31], as we have found the envelope of the resulting oscillatory pulse train to be modulated at the Q-switching frequency. Q-switching is a process in which the laser response undergoes a periodic modulation on a time scale much larger than the round-trip time, typically on the order of the geometric mean of the photon and gain medium population lifetimes in the cavity. It is caused by an alternation between two stages: one where the gain builds up for as long as the absorber can inhibit the amplification of radiation, followed by another where strong laser emission turns on and saturates the absorber, gradually depleting the gain medium back to its initial value.

Fig. 2(a) also features yet another kind of instability that manifests itself as an abrupt jump away from the destabilized state. Two such events can be observed, one at $G_0 \simeq 190$ and the other at $G_0 \simeq 240$. Remarkably enough, these jumps only occur on the two- and three-pulse branches (and form the left boundaries of their stability domains). They all lead to the fundamental-mode branch, which in contrast suffers no similar instability. This suggests a significant difference between the physical mechanisms ruling the stability of the fundamental mode and its harmonics.

In Fig. 2(b), all parameter values are the same as in Fig. 2(a) except that the round-trip time T is twice as small. This diagram shows a similar (although simpler) organization. It contains only two branches of uniform pulse trains. Again, the single-pulse branch is bounded to the left by a Q-switching instability (at $G_0 \simeq 130$), whereas the two-pulse branch features an abrupt jump to the fundamental mode-locking regime (at $G_0 \simeq 300$). One can see that the single-pulse branch in Fig. 2(b) follows very closely the two-pulse branch in Fig. 2(a). This naturally follows from the laser cavity in Fig. 2(a) being twice as long as that in Fig. 2(b), so that they can share the same mode of emission as both the fundamental mode of the shorter cavity and the second harmonic of the longer cavity. Note, however, that unlike the fundamental mode-locking regime in Fig. 2(b) the two-pulse regime shown in Fig. 2(a) does suffer a jump instability. This gives further evidence that there are qualitatively different dynamics at play determining the stability of the fundamental mode and its harmonics.

A different representation of the same dynamics is provided by Fig. 3. There, the number M of pulses, rather than the intensity maxima, is represented as a function of the unsaturated gain G_0 , showing the various transitions and hysteresis domains between the different branches of solutions. Note that the destabilized parts of those branches where the envelope of the pulsed emission patterns becomes modulated (including the quasiperiodic four-pulse regime mentioned above) are displayed as well, and are undistinguished from the uniform pulse trains in this figure. The layout of the different branches of mode-locked regimes shows the usual ramping towards higher repetition rates as a function of the pumping that has been observed in other studies [6,21,27]. For the parameter values

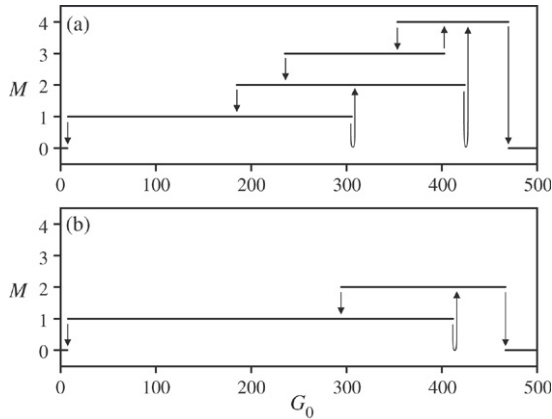


Fig. 3. Number M of pulses per round-trip as a function of the unsaturated gain G_0 , computed by the same procedure and with the same conditions as Fig. 2(a) and (b).

we chose, though, the maximum number of pulses is limited due to the relatively moderate ratio of the round-trip and filter time scales.

4. Jump instabilities

These jump instabilities deserve a closer look. Fig. 4 shows the successive intensity maxima as a function of time, during a short time window spanning the duration of the jump from the two-pulse branch to the single-pulse branch in Fig. 2(a). The successive maxima are represented as an alternation of small dots and thick dots, allowing the independent tracking of the evolutions of the two pulses in the cavity. The pattern starts out symmetric in the two pulses. Then a symmetry breaking occurs, leading to the growth and saturation of one of the pulses, and to the shrinking and vanishing of the other. The transient evolution exhibits amplified oscillations where the two pulse amplitudes oscillate in anti-phase, which is a clear indication of some interaction mechanism between them, leading to a periodic exchange of energy. The two pulses are too far apart to interact coherently via their exponentially decaying tails; nevertheless they can still interact incoherently via the gain and absorber dynamics. Such interactions, being a collective phenomenon, obviously need the coexistence of at least two pulses in the cavity to take place, and thus cannot occur within the fundamental single-pulse emission regime. Having observed no jump instability on the fundamental branch in Fig. 2, we can already foresee that pulse interactions are an essential part of the mechanism causing the jumps from the branches of higher harmonics.

The transient oscillations in Fig. 4 have a rather well-defined period. We have found it to be typically longer than the Q-switching period, and have observed that it tends to double as the spectral filter is made four times as wide, which suggests a square-root scaling law between the oscillation frequency and the pulse width. The limited information provided by the numerical data displayed in Fig. 4 alone does not enable us to understand the exact nature of the mechanism leading to these amplified oscillations, or to explain the square-root scaling law.

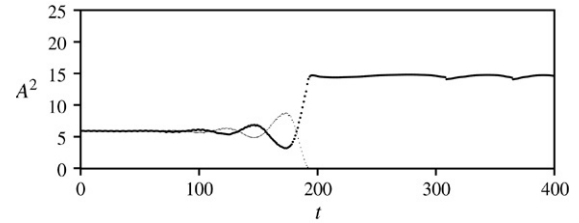


Fig. 4. Intensity maxima as a function of time, during the transition from the two-pulse branch to the single-pulse branch that occurs in Fig. 2(a) at $G_0 \simeq 190$. Successive maxima are represented alternately as thick and small dots.

The main purpose of the analysis that follows is to shed some light on these matters.

5. Analysis

The dynamics revealed by Fig. 4 features at least three distinct time scales of importance, namely: (i) the pulse width, typically on the order of magnitude of the inverse of the filter width γ ; (ii) the gain and absorber recovery times; and (iii) the duration of the jump, which extends over many round-trips. By reformulating our model equations in the limit of very narrow pulses (i.e., γT large) and a slow absorber, we shall be able to find clear relations between the different time scales.

5.1. Fast time scale: Pulse amplification

In this subsection, our goal is to obtain a system of equations that determines the shape of each emitted pulse on the $\mathcal{O}(\gamma^{-1})$ time scale and hence we define

$$\tau \equiv \gamma t. \quad (2)$$

Let us now introduce an index m , with $1 \leq m < \infty$, counting the successive instants t_m where one of the pulses hits the output mirror. Let us further define:

$$\begin{aligned} \mathcal{A}_m(t) &\equiv \gamma^{-\frac{1}{2}} A(t + t_m), & g_m(t) &\equiv g(t + t_m), \\ q_m(t) &\equiv q(t + t_m). \end{aligned} \quad (3)$$

If M is the number of pulses coexisting in the cavity, then the pulse that hits the output mirror at $t = t_m$ hits it again after one round-trip at $t = t_{m+M}$, and $t_{m+M} - t_m$ represents the corresponding round-trip time. We assume that

$$t_m - t_{m-M} \equiv T + \gamma^{-1} \delta_m, \quad (4)$$

where the constants $\gamma^{-1} \delta_m$ describe possible small deviations of the round-trip times from their cold-cavity value T . These deviations are to be determined later on in the analysis.

Substituting the relations (3) and (4) in the model equations (1) and neglecting the terms of order $\mathcal{O}(\gamma^{-1})$ in Eqs. (1b) and (1c), we arrive at the system

$$\left(1 + \frac{d}{d\tau}\right) \mathcal{A}_{m+M}(\tau - \delta_{m+M}) = \sqrt{\kappa} \exp\left[\frac{1}{2}(g_m - q_m)\right] \times \mathcal{A}_m, \quad (5a)$$

$$\frac{dg_m}{d\tau} = -\exp(-q_m) [\exp(g_m) - 1] \mathcal{A}_m^2, \quad (5b)$$

$$\frac{dq_m}{d\tau} = -s [1 - \exp(-q_m)] \mathcal{A}_m^2. \quad (5c)$$

Comparing Eqs. (1b), (1c), (5b) and (5c), one notes that we have neglected the linear terms of the former equations, which after rescaling have become of order $\mathcal{O}(\gamma^{-1})$. It reflects the fact that during the pulse emission the linear terms of Eqs. (1b) and (1c) are dominated by the nonlinear ones, because the latter are proportional to the pulse intensity A^2 .

The solutions \mathcal{A}_m of Eq. (5a) describe, for each m , the shape of the pulse that hits the output mirror for the m -th time, on a time scale τ comparable to the spectral filter width. In the limit $\gamma \rightarrow \infty$, the time τ ranges over the interval $(-\infty, \infty)$. The constants δ_m in Eq. (5a), which are so far unspecified, provide some freedom to impose constraints on the pulse shapes. A desirable requirement is that Eq. (5a) admits localized, finite-energy solutions, a condition that can be expressed as:

$$\int_{-\infty}^{+\infty} d\tau \mathcal{A}_m^2 < \infty. \quad (6)$$

It turns out that this constraint is enough to determine the constants δ_m , at least in principle. (In practice, their explicit computation is not a trivial problem without further simplifying assumptions of the kinds introduced in Sections 6 and 7.)

The system (5) is a set of delay-differential equations in τ and a set of recurrence relations in m . As a recurrence system, it is not complete. It determines the transformation of the pulse shapes after each round-trip, that is, it gives \mathcal{A}_{m+M} as a function of \mathcal{A}_m . However, it does not relate the gain and absorber state variables g_m and q_m between the passages of successive pulses, that is, for distinct values of m . The missing relations are obtained in the next subsection.

5.2. Intermediate time scale: Gain and absorber recovery

Between pulse passings, the electric field vanishes inside the gain and absorber media, which then recover exponentially according to Eqs. (1b) and (1c). More precisely, during this stage we neglect the nonlinear terms in Eqs. (1b) and (1c) by setting $A = 0$, which makes the equations linear. The limit values $g_m^\pm \equiv g_m(\tau \rightarrow \pm\infty)$ and $q_m^\pm \equiv q_m(\tau \rightarrow \pm\infty)$ of g_m and q_m obtained from Eqs. (5) represent their states right before (for the “−” sign) and right after (for the “+” sign) the m -th passing of a pulse. The exponential recovery of the gain and absorber media is expressed by

$$g_m^- - G_0 = (g_{m-1}^+ - G_0) \exp[-\gamma_g(t_m - t_{m-1})], \quad (7a)$$

$$q_m^- - Q_0 = (q_{m-1}^+ - Q_0) \exp[-\gamma_q(t_m - t_{m-1})]. \quad (7b)$$

The recovery relations (7) provide boundary conditions for the gain and absorber depletion Eqs. (5b) and (5c) and relate the gain and absorber states between successive pulse passings.

In the limit of large γ , the original model equations (1) are singular, but we have desingularized them by separating the fast time scale τ for the pulse shapes from the longer time scale for the pulse separations $t_m - t_{m-1}$, and by using Eqs. (6) and (7) as conditions on the solutions of Eqs. (5) over an infinite interval of τ . Given the first M pulse emission instants t_1, t_2, \dots, t_M as initial data, Eqs. (5)–(7) determine the complete solution profile during the first round-trip. They also supply the round-trip time

deviations δ_m , from which the next M emission instants are obtained via Eq. (4). The solution profile can then be computed for subsequent round-trips by iteration of this procedure. Eqs. (4)–(7) together thus form a well-posed problem.

5.3. Slow time scale: Pulse drift

It is possible to take advantage of the smallness of the parameter γ^{-1} that appears explicitly in Eq. (4) to emphasize the existence of a time scale much longer than the round-trip time in the system (4)–(7).

The first M pulse emission instants t_1, t_2, \dots, t_M all occur within the time window $[0, T]$, and constitute the necessary initial data for the problem (4)–(7). All the subsequent emissions are caused by the cyclic reappearance of the M initial pulses in the solution after each round-trip in the cavity. Therefore, t_{m+nM} for $1 \leq m \leq M$ and $0 \leq n < \infty$ can be thought of as the instant where the m -th pulse hits the output mirror in the cavity and is emitted for the $(n+1)$ -th time. Eq. (4) implies that successive emissions of the same pulse are separated by time intervals very close to the cold-cavity round-trip time T . We can then divide the time axis into a sequence of time intervals of duration T and consider the quantities

$$t_m^n \equiv t_{m+nM} - nT, \quad (8)$$

which, for given m and n , represent the instant of the $(n+1)$ -th emission of the m -th pulse, measured relatively to the beginning of the $(n+1)$ -th time window. In terms of those, Eq. (4) now reads

$$t_m^n - t_m^{n-1} = \gamma^{-1} \delta_m^n, \quad (9)$$

where we have defined

$$\delta_m^n \equiv \delta_{m+nM}. \quad (10)$$

Eq. (9) indicates that, in the limit $\gamma \rightarrow \infty$, the relative emission instants t_m^n for a given pulse are shifted by a very small $\mathcal{O}(\gamma^{-1})$ amount from one time window to the next. We can interpret this as a very slow drift of the pulse positions, as n increases, relatively to the parameterized time window $[nT, (n+1)T]$. This suggests looking for solutions of the system (4)–(7) where the other variables also vary little during a round-trip, and follow adiabatically these slow pulse displacements. We can write this condition compactly as

$$\mathbf{Z}_m - \mathbf{Z}_{m-M} = \mathcal{O}(\gamma^{-1}), \quad (11)$$

where \mathbf{Z}_m represents the state vector $\{\mathcal{A}_m, g_m, q_m, \delta_m\}$.

Adapting to our problem the spirit of a classical multiple scale analysis, where several copies of the time variable are introduced to describe the different scales, we now treat the round-trip index n as a slow time variable. We introduce the dimensionless variable

$$N \equiv (\gamma T)^{-1} n \quad (12)$$

and treat it as continuous rather than discrete, since it increases only by a small amount each time n is incremented by one. In

this way, we get as a limit of Eq. (9) the dynamical equation

$$\frac{dt_m(N)}{dN} = T\delta_m(N) \quad (13)$$

for the drift of the pulse positions. Consistently with our assumption that the evolution of \mathbf{Z}_m follows the pulse drift adiabatically, all quantities in the state vector \mathbf{Z}_m now must also be taken to depend on N , namely: $\mathbf{Z}_m = \mathbf{Z}_m(N)$.

Finally, we may close the infinite systems (5) and (7) by dropping the $\mathcal{O}(\gamma^{-1})$ small corrections in Eqs. (4) and (11). This gives the following periodicity conditions in m :

$$t_m(N) - t_{m-M}(N) = T, \quad \mathbf{Z}_m(N) = \mathbf{Z}_{m-M}(N), \quad (14)$$

which imply that only a finite number of variables in the system (5)–(7) are independent. Namely, the range of the index m is infinite, but every system variable can be expressed in terms of another variable with $1 \leq m \leq M$ via Eqs. (14).

Together, Eqs. (5)–(7) and (13) and (14) constitute a well-posed problem that determines the relative pulse positions $t_m(N)$ from their initial values $t_m(0)$, and henceforth we will refer to them collectively as the drift equations. They can be interpreted as a classical slow–fast system. The singular parameter γ is not contained explicitly in them, and serves only to separate the different time scales. According to Eq. (12), a unit increase in N corresponds to a number of round-trips on the order of γT , or a time scale on the order of γT^2 . The relative pulse positions t_m vary as functions of the slow variable N according to Eq. (13), and can thus be viewed as parameters of a slow motion manifold. For a given choice of the initial emission instants $t_m(0)$, Eqs. (5)–(7) together with (14) can be used to recover the complete initial solution profile in the time window $[0, T]$. This means that the fast dynamics are assumed to be already at equilibrium in this manifold of pulse solutions.

The time intervals $t_m(N) - t_{m-1}(N)$ between consecutive pulse emission instants are directly related to the separation distances between the pulses travelling in the cavity at time $t = \gamma T^2 N$. Therefore, the drift rates $\frac{dt_m}{dN}$ determined by Eq. (13) essentially measure the group velocities of the pulses. The drift equations thus describe the influence of the pulses on each other's velocities. In the two next sections, we make use of them to study the interactions between pairs of pulses and how they depend on the pulse separation.

6. Pulse interactions near threshold

The resolution of the drift equations is not a trivial problem, in particular because one of them, Eq. (5a), is a delay-differential equation and another, Eq. (6), is an integral constraint on its solutions. In this section, we make the extra assumption that the system is close to the lasing threshold. It turns out that both difficulties vanish in this case.

At the lasing threshold, the gain and absorber remain completely unsaturated, and the gain exactly compensates the combined losses from the cavity and from the absorber so that the coefficient of \mathcal{A}_m in the right-hand side of Eq. (5a) is unity. This gives the threshold condition:

$$\sqrt{\kappa} \exp\left[\frac{1}{2}(G_0 - Q_0)\right] = 1, \quad (15)$$

which defines a line in the plane (G_0, Q_0) . In a close vicinity of the threshold, the energy in one pulse is very small and the gain and absorber remain almost unsaturated during the whole pulse amplification process. From Eqs. (5b) and (5c), the depletions Δg_m and Δq_m of the gain and absorber during the passing of a pulse are given by

$$\Delta g_m = -\exp(-Q_0) [\exp(G_0) - 1] p_m + \mathcal{O}(p_m^2), \quad (16a)$$

$$\Delta q_m = -s [1 - \exp(-Q_0)] p_m + \mathcal{O}(p_m^2), \quad (16b)$$

where

$$p_m = \int_{-\infty}^{\tau} d\tau \mathcal{A}_m^2 \quad (17)$$

represents the accumulated pulse energy up to time τ . According to Eqs. (16), the net gain increase $\Delta g_m - \Delta q_m$ during the pulse emission is approximately a linear function of p_m , unless the coefficients of the linear terms in the expansions (16) are equal, in which case $\Delta g_m - \Delta q_m$ is dominated by the quadratic term in p_m . This condition reads:

$$\exp(-Q_0) [\exp(G_0) - 1] = s [1 - \exp(-Q_0)]. \quad (18)$$

Eqs. (15) and (18) together define a codimension-2 point in parameter space, which we denote $(G_0^{(0)}, Q_0^{(0)})$. The vicinity of this particular point of the threshold line is where the relevant dynamics happens. Indeed, for the pulse amplification to remain limited to a finite time window, as required for stable mode locking, the evolution of the net gain cannot be monotonous and thus must be at least quadratic in p_m .

The perturbative analysis in the vicinity of the codimension-2 point is straightforward. We introduce a formal order parameter ε measuring the distance to this point by rewriting the control parameters as $G_0 = G_0^{(0)} + \varepsilon G_0^{(1)}$ and $Q_0 = Q_0^{(0)} + \varepsilon Q_0^{(1)}$, where $\varepsilon G_0^{(1)}$ and $\varepsilon Q_0^{(1)}$ describe small deviations of G_0 and Q_0 from their reference values. We also introduce a scaled time variable $\tau = \varepsilon^{-1} \tau^{(1)}$ and the power series expansions $\mathbf{Z}_m = \mathbf{Z}_m^{(0)} + \varepsilon \mathbf{Z}_m^{(1)} + \varepsilon^2 \mathbf{Z}_m^{(2)} + \dots$, with $\mathcal{A}_m^{(0)} = 0$ so as to account for the smallness of the pulse amplitude near threshold. We carry out these substitutions in Eqs. (5)–(7) and (14), expand in powers of ε , and equate separately all the contributions of the same order in ε , obtaining a hierarchy of systems of equations. We skip the calculation details and do not write the solutions explicitly, but point out that the leading-order expressions for the pulse shapes, $\mathcal{A}_m^{(1)}$, are given by hyperbolic secants:

$$\mathcal{A}_m^{(1)} = \mathcal{A}_m^{\max} \operatorname{sech}\left(w_m^{-1} \tau^{(1)}\right), \quad (19)$$

where the amplitude maxima \mathcal{A}_m^{\max} and the width parameters w_m get determined in the course of the analysis.

A good amount of information on the dynamics in the vicinity of the codimension-2 point can be obtained from the solutions to the perturbative problem. Fig. 5 shows, in a two-parameter space, the lasing threshold line and the background instability threshold lines for the fundamental mode-locking regime and its second harmonic. Background stability means

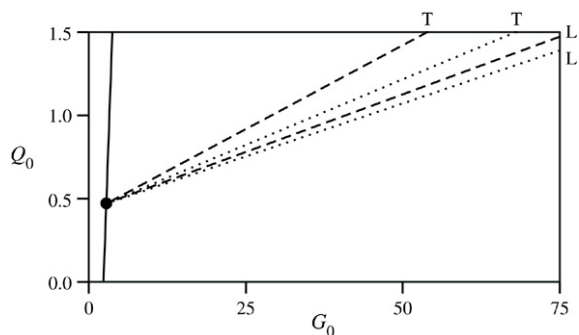


Fig. 5. Local background stability map in the vicinity of the codimension-2 point defined by Eqs. (15) and (18). Parameter values other than G_0 and Q_0 are as in Fig. 2a. The solid line is the lasing threshold, and the lines labeled T and L are respectively the trailing-edge instability threshold and the leading-edge instability threshold for the fundamental mode-locked regime (dashed lines) and its second harmonic (dotted lines).

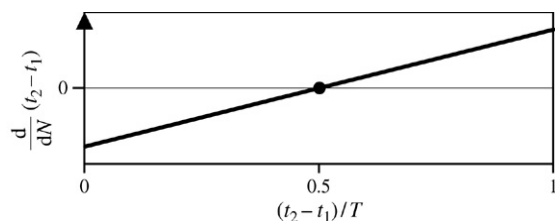


Fig. 6. Relative pulse velocity (arbitrary units) as a function of the pulse separation (in units of the cold-cavity round-trip) for a mode-locked regime with two pulses coexisting in the laser cavity. The computation is local to the codimension-2 point defined by Eqs. (15) and (18). Parameter values are $G_0 = 35$, $Q_0 = 1$, and all others as in Fig. 5.

that the net gain lies below threshold everywhere outside of the strict temporal window corresponding to the pulse emission, and is a requirement for stable mode-locked operation, especially in the presence of noise [30]. The background stability domains for the fundamental and second-harmonic mode-locked regimes are a pair of narrow, partly overlapping sectors of the (G_0, Q_0) plane that originate at the codimension-2 point. They are each bounded by a trailing edge instability line (T) and a leading edge instability line (L), where the background is marginally stable at the trailing or leading edge of the pulse, respectively. This is in agreement with Figure 3 in [30], where a different approach is used to study the model (1), showing the validity of the present approach.

Background stability alone does not guarantee a stable mode-locked operation. If several mode-locked pulses coexist inside the laser cavity, their interactions can be responsible for an instability. This is illustrated by Fig. 6, which shows, for a two-pulse regime, how the relative pulse drift velocity $\frac{d}{dN}(t_2 - t_1)$ depends on the pulse separation $t_2 - t_1$. The dot in the diagram corresponds to the configuration where the two pulses are separated by half the cavity length, leading to the emission of a regularly spaced pulse train at twice the fundamental repetition rate. This configuration is an equilibrium, because it lies on the line where the relative pulse velocity vanishes. This is a natural consequence of the symmetry of the roles played by the two pulses. The slope of the velocity curve in the vicinity of this equilibrium determines

its stability with respect to small pulse displacements. Fig. 6 shows a situation where the regular pulse train is an unstable equilibrium. Indeed, if the two pulses are brought a little closer to each other, then the sign of the relative velocity indicates that they will get even closer over time. This creates an effective attraction between the two pulses, which keeps getting stronger as the separation distance decreases. Ultimately, this leads to a collision of the pulses.

It turns out that the situation depicted in Fig. 6 is general to our model in the vicinity of the codimension-2 point. More precisely, our computations show that, in the physically relevant case where the absorber relaxes faster than the gain medium ($\gamma_q > \gamma_g$), the only possible equilibrium separation is $t_2 - t_1 = T/2$, and this equilibrium is always unstable. This result, being local, does not contradict the possibility of a stable two-pulse configuration sufficiently far away from the codimension-2 point. Nevertheless, it means that the two-pulse solution cannot be stable arbitrarily close to the threshold line, even though it could have a stable background. It must always emerge unstable at the threshold, and must undergo some bifurcation before becoming observable. This bifurcation lies outside of the domain of validity of the local approach, and its identification is the purpose of a global analysis that is carried out in the next section.

7. Pulse interactions away from threshold

Away from the codimension-2 point, the analysis of Section 6 breaks down, and therefore provides no ground for Eq. (19) anymore. Nevertheless, we assume that the pulse shape remains reasonably well approximated by a hyperbolic secant, and write: $\mathcal{A}_m \simeq \mathcal{A}_m^{\max} \text{sech}(w_m^{-1}\tau)$. Although no asymptotic argument exists to support this assumption, it has proven to give good results in practice [31]. The solution parameters \mathcal{A}_m^{\max} and w_m need to be estimated from the pulse shape Eq. (5a), along with the round-trip time deviations δ_m . To this end, we derive three independent integral relations from Eq. (5a). The following choice, although arbitrary, is a simple and reasonable possibility among others:

$$\begin{aligned} \int_{-\infty}^{\infty} d\tau L(\tau)^2 &= \int_{-\infty}^{\infty} d\tau R(\tau)^2, \\ \int_{-\infty}^{\infty} d\tau L(\tau) &= \int_{-\infty}^{\infty} d\tau R(\tau), \\ \int_{-\infty}^{\infty} d\tau \tau L(\tau) &= \int_{-\infty}^{\infty} d\tau \tau R(\tau), \end{aligned} \quad (20)$$

where $L(\tau)$ and $R(\tau)$ represent respectively the left-hand side and the right-hand side of Eq. (5a). The choice of the first of those three relations was originally motivated by its usefulness in an analysis of the original model equations (1) in the absence of filtering ($\gamma = \infty$) [31]. Also, the first two relations present the advantage that both sides of the equality are independently invariant with respect to a time translation, and are therefore independent of δ_m . This has turned out to be convenient in a study of mode-locked pulses where their velocities are not directly relevant [31].

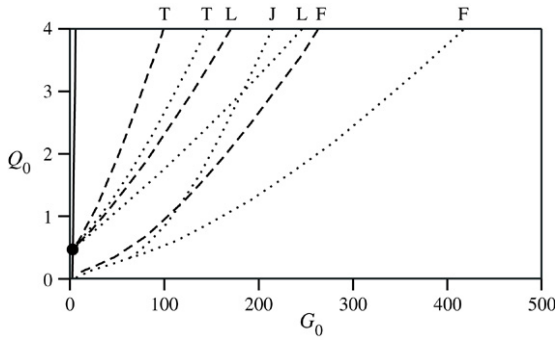


Fig. 7. Global stability map for the fundamental mode-locked regime and its second harmonic, whose bifurcations are represented as dashed lines and dotted lines, respectively. The parameter values are as in Fig. 5. The solid line is the lasing threshold. The other curves are labeled as follows: T = trailing-edge instability threshold, L = leading-edge instability threshold, F = fold (limit point) bifurcation, J = jump instability.

Substituting the hyperbolic secant ansatz $\mathcal{A}_m = \mathcal{A}_m^{\max} \operatorname{sech}(w_m^{-1} \tau)$ into Eqs. (20) gives, for all m , three conditions relating implicitly the pulse parameters \mathcal{A}_m^{\max} , w_m , and δ_m to some integral functions of the gain and absorber depletion profiles $g_m(\tau)$ and $q_m(\tau)$, which appear in Eqs. (20) through $R(\tau)$. By replacing the delay-differential equation (5a) for the pulse shape with these three conditions, we transform the system (5)–(7) and (14) into a set of ordinary differential equations for g_m and q_m with boundary and integral conditions. These equations form a simpler problem, and although they cannot be explicitly solved analytically, they can be studied using the continuation software AUTO [32].

This approach has been used to construct Fig. 7, which shows a two-parameter bifurcation diagram of the fundamental mode-locked regime and its second harmonic in the plane (G_0, Q_0) . This diagram is a global version of Fig. 5. In the vicinity of the codimension-2 point, both figures agree well. Away from the lasing threshold, Fig. 7 shows a slight curvature of the background stability threshold curves (T and L) and features some additional bifurcation curves. It is instructive to compare Fig. 7 with one of the two numerical bifurcation diagrams discussed in the beginning of this paper.

In Fig. 2(a), the stability domain of the fundamental mode-locked regime is bounded to the left by a Q-switching instability [31], and to the right by a point where the pulse peak intensity shrinks to the CW value. On the one hand, the value of G_0 at the onset of the Q-switching instability in Fig. 2(a) matches well the value of G_0 at the trailing-edge instability for $Q_0 = 4$ in Fig. 7, and indeed the proximity of these two critical values is a known fact [31]. On the other hand, the rightmost stability boundary in Fig. 2(a) can be naturally identified to one of the F curves in Fig. 7, which represent limit points where the pulse amplitude goes to zero. The numerical agreement is less good in this case, but the discrepancy is easily explained from the fact that the hyperbolic secant ansatz for the pulse shape is only an approximation, and becomes less realistic as the laser operates away from the lasing threshold. Note, finally, that the leading-edge instability curves (L) in Fig. 7 do not correspond to any remarkable event in Fig. 2(a). This means that stable mode-locked pulses can subsist even in the presence

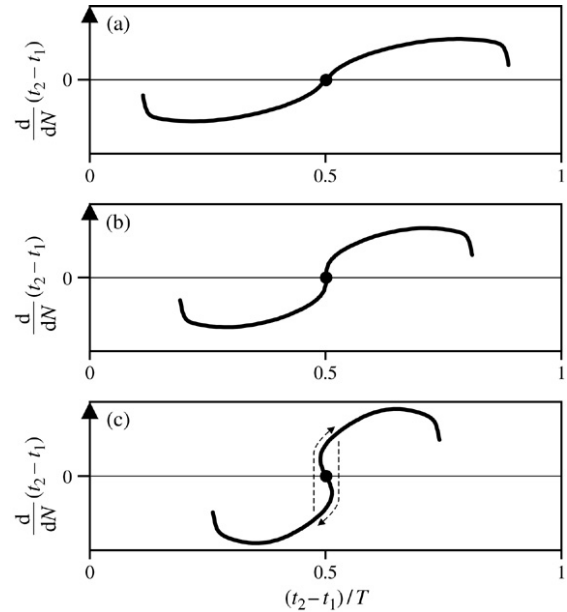


Fig. 8. Relative pulse velocity (arbitrary units) as a function of the pulse separation (in units of the cold-cavity round-trip) for a mode-locked regime with two pulses coexisting in the laser cavity. Parameter values are as in Fig. 7, with (a) $G_0 = 194.8$, (b) $G_0 = 214.8$, (c) $G_0 = 234.8$.

of an unstable background. This phenomenon, which has been reported earlier in [33,34], can occur if the relative group velocities of the pulses and of the low-intensity background are such as to sweep fluctuations towards the pulse before they get a chance to grow and alter the light wave pattern. The introduction of a weak level of noise in our model equations (1) is sufficient to oppose this effect and reveal the leading-edge instabilities in numerical simulations [30].

In addition to the bifurcations and instabilities mentioned so far, Fig. 7 features a curve labeled J, which AUTO identifies as a symmetry breaking of the second harmonic, i.e., a bifurcation to a solution that consists of two pulses with distinct shape characteristics. This symmetry breaking obviously needs the coexistence of several pulses to take place, and so it cannot manifest itself in the fundamental mode-locked regime. It can be identified as the cause of the jump that forms the leftmost boundary of the stability domain of the second harmonic branch in Fig. 2(a). The exact nature of this bifurcation is best elucidated by studying how the pulse velocities depend on the pulse separation on either side of the critical point.

Fig. 8 contains three diagrams that show, for the two-pulse regime, how the relative pulse drift velocity $\frac{d}{dN}(t_2 - t_1)$ depends on the pulse separation $t_2 - t_1$ in three different situations. Fig. 8(a), (b), (c) correspond to values of G_0 that lie respectively slightly below, just at, and slightly above the symmetry breaking point. These diagrams are similar to Fig. 6, except that they are computed using the global approach described at the beginning of this section. Again, the black dot represents an equilibrium that corresponds to the symmetric two-pulse configuration, and whose stability is indicated by the slope of the velocity curves at this point. Fig. 8 reveals that the symmetric two-pulse configuration is stable only to the right of the symmetry breaking point, in agreement with Section 6's

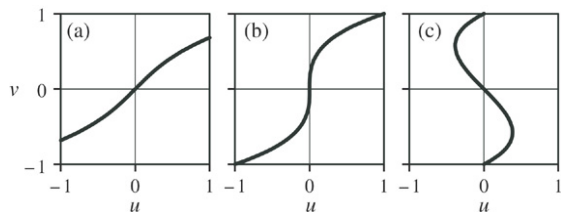


Fig. 9. Slow manifold of the van der Pol equations (21) for $\epsilon \rightarrow 0$ and (a) $\lambda = -1$, (b) $\lambda = 0$, (c) $\lambda = 1$.

conclusion that it cannot be stable arbitrarily close to the lasing threshold.

Note also the characteristic “S” shape of the velocity curve in Fig. 8(c). Because the relative velocity $\frac{d}{dt}(t_2 - t_1)$ represents the rate of change of the pulse separation as a function of the slowest time scale, this S curve can be thought of as a slow manifold similar to the one that is the main building block of the van der Pol oscillator [35]. Fig. 8(c) thus suggests the existence of a limit cycle (as indicated by the dashed arrows) that results from the interplay between a fast pulse energy relaxation dynamics and a slow pulse drift dynamics. The symmetry breaking point corresponds to a Hopf bifurcation from the symmetric two-pulse solution to this limit cycle. Fig. 8 also reveals that the bifurcation is subcritical, so the limit cycle must be unstable, and cannot be observed directly. We can show, however, that a van der Pol scenario is consistent with the onset of transient oscillations during the jump from the two-pulse branch to the single-pulse branch, which we observed in Fig. 4.

The normal form for a van der Pol limit cycle emerging from a subcritical Hopf bifurcation can be written as

$$\dot{u} = \epsilon v, \quad \dot{v} = v^3 - \lambda v - u, \quad (21)$$

where λ is the bifurcation parameter, and the small constant ϵ defines the time scale on the slow manifold. For $\lambda > 0$, Eqs. (21) are equivalent to the van der Pol equations as defined in Chap. 4 of [35] up to a rescaling and a reversal of time. Phase plane representations of the slow manifold are given in Fig. 9 for three different values of λ . Attempting a rigorous derivation of the normal form (21) from the drift equations would involve exceedingly tedious calculations. However, its validity as a description of the dynamics near the symmetry breaking point is suggested first by the strong similarity between Figs. 8 and 9, and also because the normal form (21) allows us to explain the scaling law between the transient oscillation frequency during the jump and the spectral filter width, which we mentioned at the end of Section 4. Sufficiently close to the bifurcation (i.e., for $|\lambda| \ll \epsilon$), the eigenvalues μ that determine the stability of the steady state of Eqs. (21) are given by

$$\mu = \pm i\sqrt{\epsilon} - \frac{\lambda}{2} + \mathcal{O}(\lambda^2). \quad (22)$$

For $\lambda < 0$, these eigenvalues give rise to amplified oscillations with a frequency that scales as the square root of the rate of evolution ϵ along the slow manifold. Now, remember from Eq. (12) that in our mode-locking problem, the slow time scale is proportional to the spectral filter width γ , and thus Eq. (22) predicts that the transient oscillation period P and the filter

width γ are related by $P \sim \sqrt{\gamma}$, which is consistent with observations from numerical simulations.

8. Conclusions

We have studied the effects of pulse interactions mediated by the gain and absorber dynamics in passively mode-locked lasing regimes with several coexisting, regularly spaced pulses in the laser cavity. We focused on the case of a slow absorber, and found that pulse interactions can be responsible for a particular kind of instability characterized by oscillations in the pulse energies and separation distances with a frequency that scales as the square root of the pulse width. We have identified the instability as a subcritical Hopf bifurcation to an unstable van der Pol limit cycle, thereby explaining the frequency scaling law. Due to this mechanism, stable mode-locked regimes with several coexisting pulses cannot exist arbitrarily close to the lasing threshold in our model, in contrast to the fundamental single-pulse regime.

Our findings must be contrasted with [29], where the gain dynamics in a passively mode-locked soliton laser is found to induce an effective repulsion force between adjacent solitons, which actually contributes to stabilize multiple-pulse regimes, rather than causing an instability. The reason for the disagreement is that our model and that of [29] include different physical mechanisms: pulse shaping is provided by a slow saturable absorber in our case, and by a Kerr nonlinearity in [29]. Moreover, the latter also accounts for group-velocity dispersion. The contrast between the behaviors of the two models suggests that the consequences of pulse interactions can be highly dependent on the implementation details of the particular laser system considered. In the future, this motivates further studies of pulse interactions in extended versions of the model (1) including additional physical effects.

Acknowledgements

The authors thank K. Schneider and D. Turaev for useful discussions. M. Nizette’s research is funded by the Belgian *National Fund for Scientific Research* and the Belgian *Interuniversity Attraction Pole* programme. D. Rachinskii was partially supported by the *Russian Science Support Foundation* and grants 03-01-00258, 04-01-0033 of the *Russian Foundation for Basic Research*. A. Vladimirov’s research is funded by the *Terabit Optics Berlin* project.

References

- [1] H.A. Haus, Mode-locking of lasers, *IEEE J. Sel. Top. Quantum Electron.* 6 (2000) 1173–1185; n fiber ring laser, *Phys. Rev. A* 68 (2003) 013816.
- [2] G. New, Pulse evolution in mode-locked quasi-continuous lasers, *IEEE J. Quantum Electron.* 10 (1974) 115–124.
- [3] H. Haus, Theory of mode locking with a slow saturable absorber, *IEEE J. Quantum Electron.* 11 (1975) 736–746.
- [4] F. Salin, P. Grangier, G. Rogier, A. Brun, Experimental observation of nonsymmetrical $N = 2$ solitons in a femtosecond laser, *Phys. Rev. Lett.* 60 (1988) 569–572.
- [5] M.J. Lederer, B. Luther-Davies, H.H. Tan, C. Jagadish, N.N. Akhmediev,

- J.M. Soto-Crespo, Multipulse operation of a Ti: Sapphire laser mode locked by an ion-implanted semiconductor saturable-absorber mirror, *J. Opt. Soc. Am. B* 16 (1999) 895–904.
- [6] D.Y. Tang, W.S. Man, H.Y. Tam, Stimulated soliton pulse formation and its mechanism in a passively mode-locked fibre soliton laser, *Opt. Commun.* 165 (1999) 189–194.
- [7] D.Y. Tang, W.S. Man, H.Y. Tam, P.D. Drummond, Observation of bound states of solitons in a passively mode-locked laser, *Phys. Rev. A* 64 (2001) 033814.
- [8] Ph. Grelu, F. Belhache, F. Gутty, J.-M. Soto-Crespo, Phase-locked soliton pairs in a stretched-pulse fiber laser, *Opt. Lett.* 27 (2002) 966–968.
- [9] Ph. Grelu, J. Béal, J.M. Soto-Crespo, Soliton pairs in a fiber laser: From anomalous to normal average dispersion regime, *Opt. Express* 18 (2003) 2238–2243.
- [10] D.Y. Tang, B. Zhao, D.Y. Shen, C. Lu, W.S. Man, H.Y. Tam, Compound pulse solitons in a fiber ring laser, *Phys. Rev. A* 68 (2003) 013816.
- [11] Ph. Grelu, N. Akhmediev, Group interactions of dissipative solitons in a laser cavity: The case of $2 + 1$, *Opt. Express* 12 (2004) 3184–3189.
- [12] A.N. Pilipetskii, E.A. Golovchenko, C.R. Menyuk, Acoustic effect in passively mode-locked fiber ring lasers, *Opt. Lett.* 20 (1995) 907–909.
- [13] B.A. Malomed, Bound solitons in the nonlinear Schrödinger–Ginzburg–Landau equation, *Phys. Rev. A* 44 (1991) 6954–6957.
- [14] N.N. Akhmediev, A. Ankiewicz, J.M. Soto-Crespo, Multisoliton solutions of the complex Ginzburg–Landau equation, *Phys. Rev. Lett.* 79 (1997) 4047–4050.
- [15] A.B. Grudinin, D.J. Richardson, D.N. Payne, Energy quantisation in figure eight fibre laser, *Electron. Lett.* 28 (1992) 67–68.
- [16] C. Spielmann, P.F. Curley, T. Brabec, F. Krausz, Ultrabroadband femtosecond lasers, *IEEE J. Quantum Electron.* 30 (1994) 1100–1114.
- [17] J. Ausder Au, D. Kopf, F. Morier-Genoud, M. Moser, U. Keller, 60-fs pulses from a diode-pumped Nd:glass laser, *Opt. Lett.* 22 (1997) 307–309.
- [18] M.E. Fermann, J.D. Minelly, Cladding-pumped passive harmonically mode-locked fiber laser, *Opt. Lett.* 21 (1996) 970–972.
- [19] A.B. Grudinin, S. Gray, Passive harmonic mode locking in soliton fiber lasers, *J. Opt. Soc. Am. B* 14 (1997) 144–154.
- [20] B.C. Collings, K. Bergman, W.H. Knox, True fundamental solitons in a passively modelocked short cavity Cr^{4+} :YAG laser, *Opt. Lett.* 22 (1997) 1098–1100.
- [21] B.C. Collings, K. Bergman, W.H. Knox, Stable multigigahertz pulse train formation in a short cavity passively harmonic modelocked Er/Yb fiber laser, *Opt. Lett.* 23 (1998) 123–125.
- [22] S. Sanders, A. Yariv, Passive mode locking of a two-section multiple quantum well laser at harmonics of the cavity round-trip frequency, *Appl. Phys. Lett.* 58 (1991) 681–683.
- [23] U. Bandelow, M. Radziunas, A.G. Vladimirov, B. Hüttl, R. Kaiser, 40 GHz modelocked semiconductor lasers: Theory, simulations and experiment, *Opt. Quantum Electron.* (2006) (in press).
- [24] G. Eisenstein, R.S. Tucker, U. Karen, S.K. Korotky, Active mode-locking characteristics of InGaAsP-single mode fiber composite cavity lasers, *IEEE J. Quantum Electron.* QE 22 (1986) 142–148.
- [25] J.E. Bowers, P.A. Morton, A. Mar, S.W. Corzine, Actively mode-locked semiconductor lasers, *IEEE J. Quantum Electron.* QE 25 (1989) 1426–1439.
- [26] I.N. Duling III, M.L. Dennis, Compact sources of ultrashort pulses, Cambridge Univ., Cambridge, UK, 1995.
- [27] S. Namiki, E.P. Ippen, H.A. Haus, C.X. Yu, Energy rate equations for mode-locked lasers, *J. Opt. Soc. Am. B* 14 (1997) 2099–2111.
- [28] H.A. Haus, Parameter ranges for cw passive mode locking, *IEEE J. Quantum Electron.* 12 (1976) 169–176.
- [29] J.N. Kutz, B.C. Collings, K. Bergman, W.H. Knox, Stabilized pulse spacing in soliton lasers due to gain depletion and recovery, *IEEE J. Quantum Electron.* 34 (1998) 1749–1757.
- [30] A. Vladimirov, D. Turaev, Model for passive mode locking in semiconductor lasers, *Phys. Rev. A* 72 (2005) 033808.
- [31] D. Rachinskii, A. Vladimirov, U. Bandelow, B. Hüttl, R. Kaiser, Q-switching instability in a mode-locked semiconductor laser, *J. Opt. Soc. Am. B* 23 (2006) 663–670.
- [32] <http://indy.cs.concordia.ca/auto/>.
- [33] J.L.A. Dubbeldam, J.A. Leegwater, D. Lenstra, Theory of mode-locked semiconductor lasers with finite relaxation times, *Appl. Phys. Lett.* 70 (1997) 1938–1940.
- [34] R. Paschotta, U. Keller, Passive mode locking with slow saturable absorbers, *Appl. Phys. B* 73 (2001) 653–662.
- [35] V.I. Arnol'd (Ed.), *Dynamical Systems V: Bifurcation Theory and Catastrophe Theory*, in: *Encyclopaedia of Mathematical Sciences*, Springer, 1994.